

Ultrafast X-Ray Diffraction Visualization of $B1$ - $B2$ Phase Transition in KCl under Shock Compression

Y. Y. Zhang^{1,*}, Y. X. Li^{1,*}, D. Fan,¹ N. B. Zhang,¹ J. W. Huang,¹ M. X. Tang,¹ Y. Cai,¹
X. L. Zeng,¹ T. Sun,³ K. Fezzaa,³ S. Chen,^{1,†} and S. N. Luo^{2,‡}

¹The Peac Institute of Multiscale Sciences, Chengdu, Sichuan 610207, People's Republic of China

²School of Materials Science and Engineering and School of Physical Science and Technology, Southwest Jiaotong University, Chengdu, Sichuan 610031, People's Republic of China

³Advanced Photon Source, Argonne National Laboratory, Lemont, Illinois 60439, USA



(Received 18 November 2020; revised 15 March 2021; accepted 25 June 2021; published 23 July 2021)

The classical $B1(\text{NaCl}) \leftrightarrow B2(\text{CsCl})$ transitions have been considered as a model for general structural phase transformations, and resolving corresponding phase transition mechanisms under high strain rate shock compression is critical to a fundamental understanding of phase transition dynamics. Here, we use subnanosecond synchrotron x-ray diffraction to visualize the lattice response of single-crystal KCl to planar shock compression. Complete $B1$ - $B2$ orientation relations are revealed for KCl under shock compression along $\langle 100 \rangle_{B1}$ and $\langle 110 \rangle_{B1}$; the orientation relations and transition mechanisms are anisotropic and can be described with the standard and modified Watanabe-Tokonami-Morimoto model, respectively, both involving interlayer sliding and intralayer ion rearrangement. The current study also establishes a paradigm for investigating solid-solid phase transitions under dynamic extremes with ultrafast synchrotron x-ray diffraction.

DOI: [10.1103/PhysRevLett.127.045702](https://doi.org/10.1103/PhysRevLett.127.045702)

The $B1 \leftrightarrow B2$ phase transitions occur in alkali halides [1–7] and oxides [8,9] of geophysical significance such as MgO [10–14] under isobaric heating, quasistatic compression, and shock compression. Even as the simplest first-order nondisplacive phase transitions, resolving the transition mechanisms in the $B1 \leftrightarrow B2$ transitions under shock compression has long been a challenge, which lies in ultrafast visualization of lattice response during highly transient shock events (hundreds nanoseconds or less) [1,5]. KCl is a model material for studying the $B1 \leftrightarrow B2$ phase transitions because of its relatively low transition pressure (~ 2 GPa) [15]. A multitude of transition mechanisms were proposed for the $B1 \leftrightarrow B2$ transitions [7,16–27], and a notable mechanism is the Watanabe-Tokonami-Morimoto (WTM) model, which involves a concerted translation of adjacent $(100)_{B1}$ lattice planes relative to one another with simultaneous rearrangements of the ions within each plane [7]. A model based on high-speed dislocations was also proposed for the shock-induced $B1$ - $B2$ transition in KCl [17], but disputed by a follow-up study [1]. Dynamic x-ray diffraction (XRD) with flash x rays was applied to single-crystal KCl under shock compression [1,5]; nonetheless, the results are inconclusive regarding the $B1$ - $B2$ transition mechanisms. Overall, such questions as the exact transition mechanisms, the existence of general mechanisms and anisotropy, and the effects of stress or loading conditions, remain open. The key issues in previous dynamic XRD experiments on the shock-induced $B1$ - $B2$ transition mechanisms are the extreme paucity of

dynamic XRD data and the lack of sufficient Laue diffraction spots on a single XRD pattern to constrain crystallographic orientation relations between the parent and daughter phases.

Here, we report lattice-scale visualization of the $B1$ - $B2$ phase transition in $[110]_{B1}$ - and $[100]_{B1}$ -oriented single-crystal KCl under shock compression with ultrafast synchrotron x-ray diffraction, which reveals full crystallographic orientation relations between the $B1$ and $B2$ phases. The $B1$ - $B2$ orientation relations for $[100]_{B1}$ -oriented KCl are consistent with the standard WTM model; however, different orientation relations are observed for $[110]_{B1}$ -oriented KCl and can be explained with a modified WTM model: a new model of the $B1$ - $B2$ transition based on the $\{110\}_{B1}$ translation and intralayer atomic displacement.

The experimental setup for *in situ* ultrafast Laue x-ray diffraction measurements under shock compression loading is shown schematically in Fig. 1(a) (see Sec. S2 in the Supplemental Material [28] for details) [43]. Shock compression is achieved via plate impact with a two-stage light gas gun installed at beam line 32-ID-B of the Advanced Photon Source (APS), Argonne National Laboratory, USA. White x rays with narrow-banded harmonics from an undulator insertion device are used for x-ray diffraction measurements (Fig. S1 in the Supplemental Material [28]). Plate impact provides a well-defined uniaxial strain loading condition within the shocked sample, and transient x-ray diffraction measures directly lattice response to shock

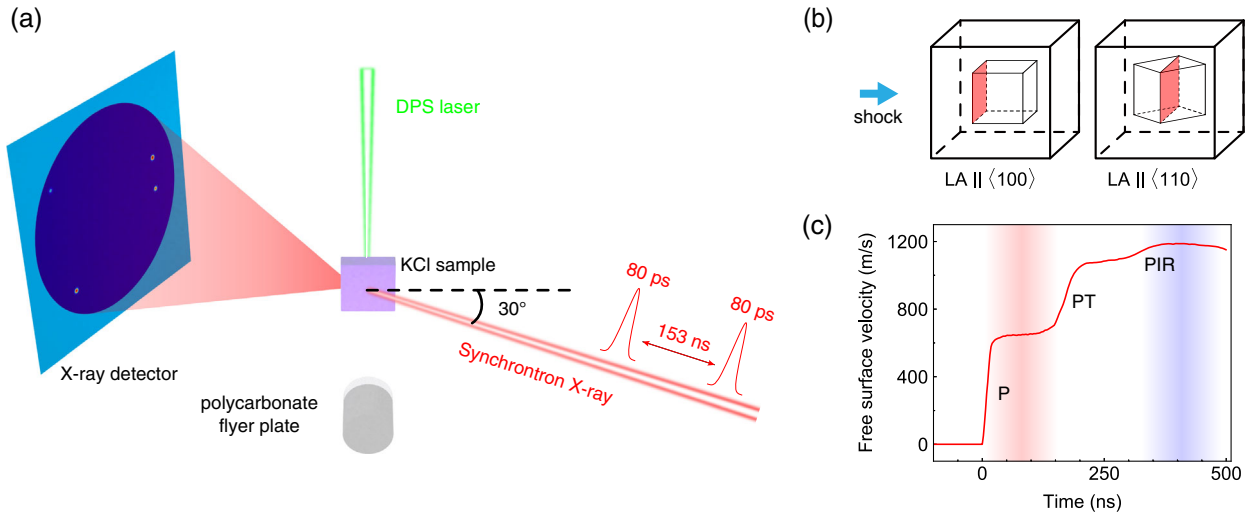


FIG. 1. Schematic of experimental setup. (a) Gas-gun shock compression loading with sub-ns x-ray diffraction measurements (see Sec. S2 in the Supplemental Material [28] for details). The probe x-ray pulse width is approximately 80 ps, and the pulse interval is about 153 ns. DPS: Doppler pin system or Doppler laser interferometry. (b) $[110]_{B1}$ - and $[100]_{B1}$ -oriented single-crystal KCl targets. The impact loading axis (LA) is perpendicular to the $(110)_{B1}$ or $(100)_{B1}$ lattice plane (red). (c) Representative free-surface velocity history of the $[110]_{B1}$ target measured with DPS, showing a plastic wave (P), a phase transition wave (PT), and a phase interface reflection wave (PIR) [45]. Here, time zero refers to the shock breakout at the free surface.

compression, including phase transitions. $[110]_{B1}$ - and $[100]_{B1}$ -oriented KCl single crystals [Fig. 1(b)] are shock-compressed and probed with synchrotron x-rays to obtain time-resolved XRD patterns before and after the phase transition. The exposure time for an XRD pattern is about 80 ps (full-width at half maximum or FWHM of the temporal profile of an x-ray pulse), which also represents the highest temporal resolution allowed for such single-bunch, single-shot, measurements based on storage-ring-type synchrotron radiation. A Doppler laser interferometer system (Doppler pin system) [44] is implemented to record free-surface velocity histories. A typical free-surface velocity history is shown in Fig. 1(c) for an impact velocity of 1578 m s^{-1} .

Representative two-dimensional diffraction patterns for shock loading along $[110]_{B1}$ are shown in Fig. 2. As a result of the transmission diffraction geometry and the inherent bandwidth of the white undulator x-ray source, sufficient diffraction spots are captured to ensure the accurate determination of crystal orientations. At ambient conditions (referred to as static), four main Laue diffraction spots are observed, three of which each have a secondary spot, due to misorientation in the imperfect “single-crystal” KCl sample of the $B1$ phase. Broadening of the diffraction spots is minor, indicating negligible internal strain and defects except low-angle grain boundaries. The static Laue diffraction spots are indexed, and the normal of the sample impact surface is of the crystallographic $[110]_{B1}$ orientation as expected [Fig. 2(a)]. Corresponding single-crystal Laue diffraction simulation matches well the measured pattern [Fig. 2(b)].

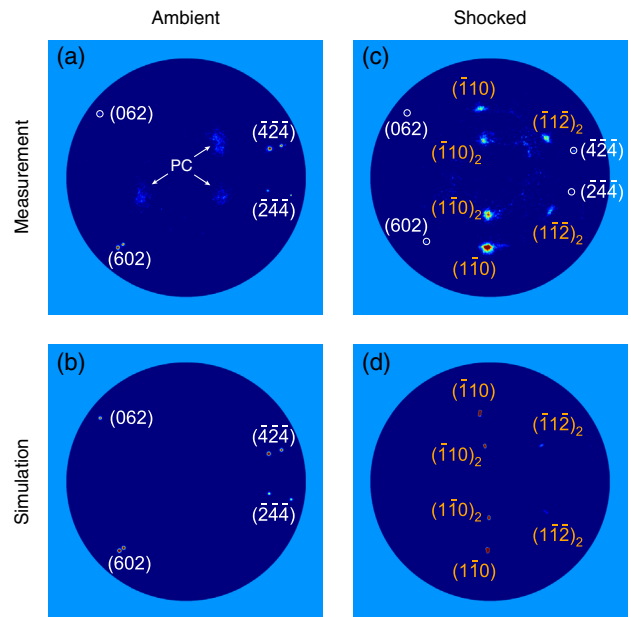


FIG. 2. Shock compression of single-crystal KCl along $[110]_{B1}$. (a) Measured static XRD pattern of the $B1$ phase before impact. (b) Simulated static XRD pattern of the $B1$ phase corresponding to (a). (c) Measured dynamic XRD pattern (323 ns after impact), showing diffraction spots from both the $B1$ and $B2$ phases. (d) Simulated dynamic XRD pattern of the $B2$ phase corresponding to (c). Diffraction spots from the $B1$ phase are not shown in (d) for clarity. White Miller indices: the $B1$ phase; orange Miller indices: the $B2$ phase. Subscript 2: diffraction spots due to the second harmonic of the synchrotron undulator source. White circles: low-intensity spots. PC: scattered x rays from the polycarbonate projectile and windows.

Upon shock compression, both the free-surface velocity history [Fig. 1(c)] and the Laue diffraction pattern [Fig. 2(c)] demonstrate the $B1$ - $B2$ phase transition in KCl. The three-wave structure, consisting of a plastic wave, a phase transition wave and a phase interface reflection wave [45], is identified from the free-surface velocity history [Fig. 1(c)], consistent with previous measurements [46]. The corresponding peak shock stress is approximately 3 GPa. On the dynamic Laue XRD pattern [Fig. 2(c)], the intensities of the original four main diffraction spots decrease partly due to the reduction in volume fraction of the preexisting $B1$ phase, while the secondary spots disappear owing to the shock-induced lattice deformation. Six new Laue spots appear as a result of the $B1$ - $B2$ phase transition.

To determine the Miller indices of the newly emerged Laue spots on a dynamic XRD pattern, we conduct diffraction pattern analysis and forward Laue x-ray diffraction simulation using the corresponding x-ray spectrum from the undulator source (Fig. S1 in the Supplemental Material [28]). Corresponding Miller indices are shown in Fig. 2(c). Four $\{110\}$ spots and two $\{112\}$ spots are identified. Here, the two $\{110\}$ spots with the same azimuthal angles but different diffraction angles are attributed to the fundamental and the second harmonic (denoted with subscript 2) of the probe x-ray spectrum. A pair of such spots with the same Miller indices are not expected on the same detector plane for an ideal single crystal; the appearance of the two $\{110\}$ pairs, $(\bar{1}10)$ and $(\bar{1}10)_2$, and $(1\bar{1}0)$ and $(1\bar{1}0)_2$, indicates that the $B2$ phase induced by the shock compression is a highly textured single crystal with a certain crystal orientation distribution, i.e., polycrystallization. The difference in diffraction angle between the adjacent $\{110\}$ spots is about 5° , corresponding to a misorientation range of $\sim 2.5^\circ$. Such polycrystallization of the daughter phase is common in the $B1 \leftrightarrow B2$ phase transitions of alkali halides under quasistatic compression or isobaric heating [6,7,23], and it is more pronounced than in the dynamic compression due to the differences in stress condition and timescale involved [5]. The two new $\{112\}_2$ spots are from the second harmonic. The simulated Laue diffraction pattern of the $B2$ phase under shock compression is obtained [Fig. 2(d)] considering the orientation distribution and the first two harmonics of the x-ray spectrum, and is in excellent agreement with the measured dynamic pattern in Fig. 2(c).

The Laue diffraction spots are well identified for the $B1$ and $B2$ phases on the static and dynamic diffraction patterns, allowing for the determination of the entire crystallographic orientation relations between the $B1$ and $B2$ phases for shock compression along $[110]_{B1}$ (see Sec. S3B in the Supplemental Material [28] for details), as represented by the three basic crystallographic orientations in each phase, i.e.,

$$\begin{cases} [110]_{B1} \parallel [\bar{1}\bar{1}2]_{B2} \\ [001]_{B1} \parallel [111]_{B2} \\ [1\bar{1}0]_{B1} \parallel [\bar{1}10]_{B2} \end{cases} \quad (1)$$

This set of the $B1$ - $B2$ orientation relations is complete for $[110]_{B1}$ -oriented KCl, and has not been previously observed in shock compression experiments. It also has a mirrored counterpart (see Eq. S6 in the Supplemental Material [28]).

For $[100]_{B1}$ -oriented KCl, our dynamic XRD measurement also yields the first complete $B1$ - $B2$ orientation relations upon shock compression (see Sec. S4 in the Supplemental Material [28] for details). Two sets of orientation relations are identified as

$$\begin{cases} [100]_{B1} \parallel [110]_{B2} \\ [010]_{B1} \parallel [\bar{1}11]_{B2} \\ [001]_{B1} \parallel [1\bar{1}2]_{B2} \end{cases}, \text{ and } \begin{cases} [100]_{B1} \parallel [110]_{B2} \\ [010]_{B1} \parallel [\bar{1}\bar{1}2]_{B2} \\ [001]_{B1} \parallel [\bar{1}11]_{B2} \end{cases} \quad (2)$$

The $B1$ - $B2$ orientation relations exhibit a strong anisotropy as seen for $[100]_{B1}$ - and $[110]_{B1}$ -oriented KCl under shock compression. Given the orientation relations resolved from our experiments, we search for possible mechanisms for the shock-induced $B1$ - $B2$ phase transition. Various models have been proposed for the $B1 \leftrightarrow B2$ phase transitions. For example, the classical Buerger model [16] involves contraction along $\langle 111 \rangle_{B1}$, and thus requires a common $\langle 111 \rangle$ crystallographic direction for both the $B1$ and $B2$ structures, which nonetheless contradicts the observed orientation relations for both the $[110]_{B1}$ and $[100]_{B1}$ shock loading cases.

The standard WTM model involves interlayer sliding between and intralayer ion rearrangement on the $(100)_{B1}$ planes [7]. Another model by Gufan and Ternovskii involves parallel shift of and corresponding intralayer ion rearrangement on the $(100)_{B1}$ planes [21]. These two models yield orientation relations consistent with the measurement in the $[100]_{B1}$ shock loading case but not in the $[110]_{B1}$ case. Fraser and Kennedy proposed a series of models based on the martensitic transformation [18,19], and their type-1 and 3 models can reproduce the observed orientation relations in the $[100]_{B1}$ and $[110]_{B1}$ loading cases, respectively.

To better understand the phase transition mechanisms, we conduct molecular dynamics (MD) simulations of shock compression of $[100]_{B1}$ - and $[110]_{B1}$ -oriented KCl single crystals (Figs. S6 and S9 [28]). On the basis of the MD simulations and the measured orientation relations, we propose a modified WTM model for the shock-induced $B1$ - $B2$ transition in KCl. (The models by Fraser and Kennedy conflict with the MD simulations [28] and are thus discarded.) The modified WTM model involves interlayer sliding and intralayer rearrangement of ions as

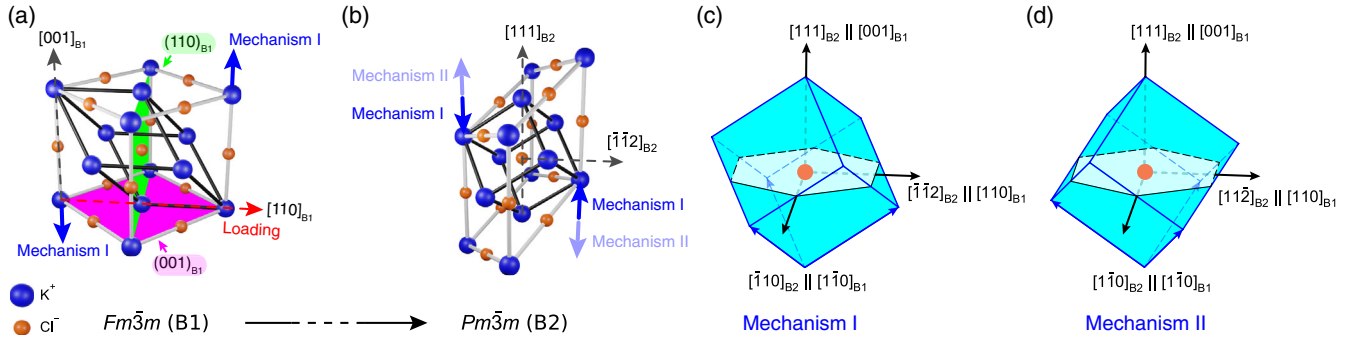


FIG. 3. $B1 \rightarrow B2$ phase transition mechanisms in single-crystal KCl under shock compression along $[110]_{B1}$. (a) Initial crystal structure of the $B1$ phase. The virtual $B2$ unit cell within the $B1$ lattice is indicated in black lines. (b) Resultant structure of the $B2$ phase. The $B2$ unit cell is indicated in black lines. (c) and (d) Crystal structures of the $B2$ phase for mechanisms I and II, respectively. Blue: K^+ ; orange: Cl^- . Arrows: sliding directions.

the standard WTM model. However, the standard WTM model only allows for the $(100)_{B1}$ sliding planes, while in the modified WTM model, different sliding planes [the $(110)_{B1}$ planes] are involved.

For shock along $[100]_{B1}$, the $B1$ - $B2$ transition can be explained with the standard WTM model as detailed in Sec. S3 of Supplemental Material [28]. For shock along $[110]_{B1}$, a modified WTM model is proposed: a new model of the $B1$ - $B2$ transition based on the $(110)_{B1}$ translation and intralayer atomic displacement. Figures 3(a) and 3(b) show the initial and final lattice structures of the $B1$ and $B2$ phases, respectively. The cell structures drawn in black lines represent the virtual $B2$ “unit cell” in the original $B1$ phase [Fig. 3(a)] and in the $B2$ unit cell [Fig. 3(b)]. Here, the sliding planes are consecutive $(110)_{B1}$ planes, rather than the $(100)_{B1}$ planes as proposed in the standard WTM model [1,7].

Considering the symmetry of the $B1$ structure under the $[110]_{B1}$ loading, there are two mechanisms with opposite sliding directions. For any $(110)_{B1}$ plane, its two immediately adjacent $(110)_{B1}$ planes slide along $\pm[001]_{B1}$, respectively (mechanism I), or in opposite directions, $\mp[001]_{B1}$ (mechanism II). Along with the interlayer sliding, intralayer ion rearrangement on the $(110)_{B1}$ planes leads to the formation of the $B2$ structure. Detailed interlayer sliding and intralayer ion rearrangement are shown in Fig. S5. Consequently, the complete orientation relations corresponding to these transition mechanisms are obtained [Figs. 3(c) and 3(d)], and those for mechanism I are identical to our experimental results [Eq. (1)]. Therefore, the standard and modified WTM mechanism can explain the $[100]_{B1}$ and $[110]_{B1}$ shock loading cases, respectively, as well as the MD simulations.

The shocked KCl single crystals show anisotropy in the exact $B1$ - $B2$ phase transition mechanisms. High strain rate planar shock loading induces a uniaxial strain or nonhydrostatic condition, and the inherent crystallographic anisotropy of single crystal KCl combined with non-hydrostatic stress, i.e., the structure and loading

anisotropies lead to the observed anisotropy in transition mechanism.

Numerous models have been proposed for the extensively studied $B1 \leftrightarrow B2$ phase transitions under nonshock loading conditions [16,18–27] (Sec. S5 in the Supplemental Material [28]), and some models present intermediate phase(s) along the transition pathways. However, no consensus has been reached on mechanisms or intermediate phases. It is highly desirable to directly measure intermediate phases. In our shock experiments on KCl single crystals, only the initial $B1$ and final $B2$ phases are manifested in the diffraction patterns, and the phase transition shock wave front in the free-surface velocity histories with a nanosecond temporal resolution [PT in Figs. 1(c) and S3 in the Supplemental Material [28]] shows no splitting, i.e., no indication of an intermediate phase. The intermediate phase in the narrow shock front of the phase transition wave constitutes a minor volume fraction of the total volume sampled by x rays, and thus has a negligible contribution to the diffraction intensity. A well-defined intermediate phase cannot be identified from the MD trajectories, either, likely as a result of the extreme strain rate and small system size inherently involved in MD simulations.

Intermediate phases appear to be highly elusive during the shock-induced $B1$ - $B2$ transition in KCl, and one may have to resort to other novel ultrafast loading and diagnostic means to address the challenge of capturing such phases. For instance, short-pulse laser shock loading combined with ultrafast x-ray or electron diffraction [47–49] can be exploited to capture intermediate structures just around the phase transition wave front, and the transition pathways can be constrained or identified. In addition, the kinetics of $B1$ - $B2$ phase transition is directly relevant to the exact transition pathways and the lifetime of an intermediate phase (thus its detection), and depends on strain rate [50], stress state [50], defects [17,50,51], and species (alkali halides and chalcogenides), which should be explored systematically in the future regarding KCl in particular and other materials in general.

The current study advances our understanding of the transition mechanisms of the $B1 \leftrightarrow B2$ phase transitions in single crystals under shock compression in particular, and bears significant implications to structural phase transitions under extreme conditions in general. Our ultrafast XRD measurements along with molecular dynamics simulations present a distinct and exciting opportunity to examine and understand the fundamental atomistic mechanisms that underlie shock-induced phase transition in unprecedented detail. This study also establishes a paradigm for investigating structural phase transitions [48,52–55] in highly transient events including high-pressure and high strain-rate phenomena of significance in planetary science, condensed matter physics, inertial confinement fusion, and additive manufacturing.

This work was partially supported by the Scientific Challenge Project of China (Grant No. TZ2018001), and NSFC (Grant No. 11627901). Use of the Advanced Photon Source, an Office of Science User Facility operated for the US Department of Energy (DOE) Office of Science by Argonne National Laboratory, was supported by the US DOE under Contract No. DE-AC02-06CH11357.

*These authors contributed equally to this work.

†schen@pims.ac.cn

*sluo@swjtu.edu.cn

- [1] T. d'Almeida and Y. M. Gupta, *Phys. Rev. Lett.* **85**, 330 (2000).
- [2] E. Knittle and R. Jeanloz, *Science* **223**, 53 (1984).
- [3] D. Zahn and S. Leoni, *Phys. Rev. Lett.* **92**, 250201 (2004).
- [4] L. Hautala, K. Jänkälä, T. Löytynoja, M.-H. Mikkeli, N. Prisle, M. Tchapyguine, and M. Huttula, *Phys. Rev. B* **95**, 045402 (2017).
- [5] S. J. Turneaure, Y. M. Gupta, and P. Rigg, *J. Appl. Phys.* **105**, 013544 (2009).
- [6] B. Okai, *J. Phys. Soc. Jpn.* **48**, 514 (1980).
- [7] M. Watanabe, M. Tokonami, and N. Morimoto, *Acta Crystallogr. Sec. A* **33**, 294 (1977).
- [8] R. Jeanloz, T. J. Ahrens, H. K. Mao, and P. M. Bell, *Science* **206**, 829 (1979).
- [9] H. Ozawa, F. Takahashi, K. Hirose, Y. Ohishi, and N. Hirao, *Science* **334**, 792 (2011).
- [10] S. Root, L. Shulenburg, R. W. Lemke, D. H. Dolan, T. R. Mattsson, and M. P. Desjarlais, *Phys. Rev. Lett.* **115**, 198501 (2015).
- [11] R. S. McWilliams, D. K. Spaulding, J. H. Eggert, P. M. Celliers, D. G. Hicks, R. F. Smith, G. W. Collins, and R. Jeanloz, *Science* **338**, 1330 (2012).
- [12] F. Coppari, R. F. Smith, J. H. Eggert, J. Wang, J. R. Rygg, A. Lazicki, J. A. Hawreliak, G. W. Collins, and T. S. Duffy, *Nat. Geosci.* **6**, 926 (2013).
- [13] T. Sekine, N. Ozaki, K. Miyaniishi, Y. Asaumi, T. Kimura, B. Albertazzi, Y. Sato, Y. Sakawa, T. Sano, S. Sugita, T. Matsui, and R. Kodama, *Sci. Adv.* **2**, e1600157 (2016).
- [14] J. Bouchet, F. Bottin, V. Recoules, F. Remus, G. Morard, R. M. Bolis, and A. Benuzzi-Mounaix, *Phys. Rev. B* **99**, 094113 (2019).
- [15] P. W. Bridgman, *Proc. Am. Acad. Arts Sci.* **76**, 1 (1945).
- [16] M. J. Buerger, *Phase Transitions in Solids* (Wiley, New York, 1951), p. 183.
- [17] E. Zaretsky, *J. Phys. Chem. Solids* **59**, 253 (1998).
- [18] W. L. Fraser and S. W. Kennedy, *Acta Crystallogr. Sect. B* **28**, 3101 (1972).
- [19] W. L. Fraser and S. W. Kennedy, *Acta Crystallogr. Sec. A* **30**, 13 (1974).
- [20] K. Knorr, L. Ehm, M. Hytha, B. Winkler, and W. Depmeier, *Eur. Phys. J. B—Condens. Matter* **31**, 297 (2003).
- [21] Y. M. Gufan and I. Ternovskii, *Phys. Solid State* **35**, 639 (1993).
- [22] H. Sowa, *Acta Crystallogr. Sect. A* **56**, 288 (2000).
- [23] P. Tolédano, K. Knorr, L. Ehm, and W. Depmeier, *Phys. Rev. B* **67**, 144106 (2003).
- [24] A. G. Christy, *Acta Crystallogr. Sect. B* **49**, 987 (1993).
- [25] A. Grzechnik and K. Friese, *J. Phys. Condens. Matter* **22**, 095402 (2010).
- [26] H. T. Stokes and D. M. Hatch, *Phys. Rev. B* **65**, 144114 (2002).
- [27] H. T. Stokes, D. M. Hatch, J. Dong, and J. P. Lewis, *Phys. Rev. B* **69**, 174111 (2004).
- [28] See Supplemental Material at <http://link.aps.org/supplemental/10.1103/PhysRevLett.127.045702> for additional details on experiments, Laue pattern indexing, x-ray diffraction simulations, molecular dynamics simulations, and phase transition mechanisms, which includes Refs. [29–42].
- [29] M. Sánchez del Río and R. J. Dejus, *Proc. SPIE Int. Soc. Opt. Eng.* **5536**, 171 (2004).
- [30] S. N. Luo, B. J. Jenson, D. E. Hooks, K. Fezzaa, K. J. Ramos, J. D. Yeager, K. Kwiatkowski, and T. Shimada, *Rev. Sci. Instrum.* **83**, 073903 (2012).
- [31] D. Fan, J. W. Huang, X. L. Zeng, Y. Li, J. C. E. J. Y. Huang, T. Sun, K. Fezzaa, Z. Wang, and S. N. Luo, *Rev. Sci. Instrum.* **87**, 053903 (2016).
- [32] V. K. Gupta and S. R. Agnew, *J. Appl. Crystallogr.* **42**, 116 (2009).
- [33] G. Will, *Fortschritte Mineral.* **59**, 31 (1981).
- [34] D. Walker, P. K. Verma, L. M. Cranswick, R. L. Jones, S. M. Clark, and S. Buhre, *Am. Mineral.* **89**, 204 (2004).
- [35] J. W. Huang, Y. Y. Zhang, S. C. Hu, Y. Cai, and S. N. Luo, *J. Appl. Crystallogr.* **54**, 686 (2021).
- [36] S. Plimpton, *J. Comp. Phys.* **117**, 1 (1995).
- [37] X. W. Zhou, F. P. Doty, and P. Yang, *Comput. Mater. Sci.* **50**, 2470 (2011).
- [38] P. M. Larsen, S. Schmidt, and J. Schiøtz, *Model. Simul. Mater. Sci. Eng.* **24**, 055007 (2016).
- [39] A. Stukowski, *Model. Simul. Mater. Sci. Eng.* **18**, 015012 (2010).
- [40] R. Hielscher and H. Schaeben, *J. Appl. Crystallogr.* **41**, 1024 (2008).
- [41] D. Mainprice, F. Bachmann, R. Hielscher, and H. Schaeben, *Geol. Soc. Lond. Spec. Publ.* **409**, 251 (2015).
- [42] S. Zhang and N. X. Chen, *Acta Mater.* **51**, 6151 (2003).
- [43] S. Chen, Y. X. Li, N. B. Zhang, J. W. Huang, H. M. Hou, S. J. Ye, T. Zhong, X. L. Zeng, D. Fan, L. Lu, L. Wang,

- T. Sun, K. Fezzaa, Y. Y. Zhang, M. X. Tang, and S. N. Luo, *Phys. Rev. Lett.* **123**, 255501 (2019).
- [44] O. T. Strand, D. R. Goosman, C. Martinez, T. L. Whitworth, and W. W. Kuhlow, *Rev. Sci. Instrum.* **77**, 083108 (2006).
- [45] L. M. Barker and R. E. Hollenbach, *J. Appl. Phys.* **45**, 4872 (1974).
- [46] J. C. Boettger and D. C. Wallace, *Phys. Rev. B* **55**, 2840 (1997).
- [47] C.-Y. Ruan, F. Vigliotti, V. A. Lobastov, S. Chen, and A. H. Zewail, *Proc. Natl. Acad. Sci. U.S.A.* **101**, 1123 (2004).
- [48] S. J. Turneaure, N. Sinclair, and Y. M. Gupta, *Phys. Rev. Lett.* **117**, 045502 (2016).
- [49] S. Vogelgesang, G. Storeck, J. G. Horstmann, T. Diekmann, M. Siviš, S. Schramm, K. Rossnagel, S. Schäfer, and C. Ropers, *Nat. Phys.* **14**, 184 (2018).
- [50] J. W. Christian, *The Theory of Transformations in Metals and Alloys* (Pergamon, London, 2002).
- [51] I. Ruff, A. Baranyai, E. Spohr, and K. Heinzinger, *J. Chem. Phys.* **91**, 3148 (1989).
- [52] D. H. Kalantar, J. F. Belak, G. W. Collins, J. D. Colvin, H. M. Davies, J. H. Eggert, T. C. Germann, J. Hawreliak, B. L. Holian, K. Kadau, P. S. Lomdahl, H. E. Lorenzana, M. A. Meyers, K. Rosolankova, M. S. Schneider, J. Sheppard, J. S. Stölken, and J. S. Wark, *Phys. Rev. Lett.* **95**, 075502 (2005).
- [53] S. J. Turneaure, S. M. Sharma, T. J. Volz, J. M. Winey, and Y. M. Gupta, *Sci. Adv.* **3**, eaao3561 (2017).
- [54] S. Wall, S. Yang, L. Vidas, M. Chollet, J. M. Glowia, M. Kozina, T. Katayama, T. Henighan, M. Jiang, T. A. Miller, D. A. Reis, L. A. Boatner, O. Delaire, and M. Trigo, *Science* **362**, 572 (2018).
- [55] E. E. McBride, A. Krygier, A. Ehnes, E. Galtier, M. Harmand, Z. Konôpková, H. J. Lee, H. P. Liermann, B. Nagler, A. Pelka, M. Rödel, A. Schropp, R. F. Smith, C. Spindloe, D. Swift, F. Tavella, S. Toleikis, T. Tschentscher, J. S. Wark, and A. Higginbotham, *Nat. Phys.* **15**, 89 (2019).